Bioimpedance Spectroscopy

Klösgen, Beate; Rümenapp, Christine; Gleich, Bernhard

Published in:
BetaSys

DOI:
10.1007/978-1-4419-6956-9

Publication date:
2011

Document Version
Final published version

Chapter 11
Bioimpedance Spectroscopy

Beate Klösgen, Christine Rümenapp, and Bernhard Gleich

Abstract In the context of biology, electrical phenomena are usually identified with ionic currents through protein channels, for example as they are postulated during nerve signalling (Andersen et al. Prog Neurobiol 88(2):104–113, 2009; Sakmann and Neher Annu Rev Physiol 46:455–472, 1984). However, there are more electrical phenomena that play a significant role in biological systems, namely those arising from polarization effects (Grimnes Bioimpedance and Bioelectricity, 2008; Polk Handbook of Biological Effects of Electromagnetic Fields 1996). Local inhomogeneities in charge distributions give rise to the formation of permanent molecular dipoles as in uncharged molecules such as (hydration) water, or due to the polar groups in proteins and lipid molecules. Non-permanent electrical dipoles can originate from the presence of ions in solution. Structured distributions of counter-ions at all polar interfaces, for example along the surface of proteins and especially along the polar membrane interfaces of cells, cause the formation of Stern and Helmholtz layers. All non-uniform distributions of charges and dipoles initiate and modify internal local electrical fields. Moreover, the application of external fields causes relaxation processes with characteristic contributions to the frequency-dependent complex dielectric constant. These dipolar relaxations were initially described by Debye (Polare Molekeln 1929). They are the basis of impedance spectroscopy (K'Owino and Sadik Electroanalysis 17(23):2101–2113, 2005; Schwan Adv-Biol-and-Med-Phys (5):147–209, 1957; Schwan et al. J Phys Chem 66(12):2626–2635, 1962). The dispersion and the related adsorption contributions of the dielectric spectrum yield the dipole-specific relaxation frequencies and also give information about the dipole density. Redistributions of dipoles, binding events and changes in local viscosity will all appear as modifications of the signal amplitude and in system-specific frequency shifts. These changes in the measured spectra can be used in a variety of technical devices, for example for biosensing as well as for monitoring the properties of cells in cell culture.

B. Klösgen (✉)
Institute for Physics and Chemistry and MEMHYS – Center for Biomembrane Physics,
University of Southern Denmark, Campusvej 55, 5340 Odense M, Denmark
e-mail: kloesgen@ifk.sdu.dk

B. Booß-Bavnbek et al. (eds.), *BetaSys*, Systems Biology 2,
DOI 10.1007/978-1-4419-6956-9_11, © Springer Science+Business Media, LLC 2011

Keywords Impedance spectroscopy · Dielectric relaxation spectroscopy · Lab-on-a-chip · Biosensor

11.1 Introduction

Non-invasive techniques for the investigation of complex processes such as the monitoring of chemical reactions and changes of composition and shapes are considered attractive tools in many areas of science and engineering and especially for medical applications. Among the early options, the in vitro and even in vivo investigation of electrical properties of materials was identified as a potential tool for non-invasive methods: apparatus were seemingly simple and ready at hand, consisting essentially of power supplies and electrodes. The acquisition of electroencephalograms or electrocardiograms is nowadays standard in medical diagnosis. Still, electrodes may be considered in a more general way as a tool either for the injection of currents into biomaterial with the goal of measuring impedance responses or for the application of fields to investigate dielectric polarization responses. These two apparently different methods address two aspects of the same phenomenon, namely the frequency-dependent complex dielectric constant that is a material property of specific constituents, composition and geometry and micro-surroundings.

At zero field frequency, in the case of a so-called direct current (DC) situation, the electrical properties of the material are essentially represented by the Ohm resistance with its specific conductivity due to mobile charges. The dielectric properties are hidden in the presence of the passive capacitance due to interfacial charge accumulation and dipole alignment within the dielectricum. They only show up during the switching-on or switching-off process (see Section 11.2.5.1) but do not contribute to the steady current (DC).

At very high frequency, in the case of an AC situation, the dielectric properties are reflected in the complex refractive index, consisting of a dispersion (real) and an absorption (imaginary) part. The relative impact of conductivity versus dipole orientation is shifted as frequency increases. Therefore, DC resistance is replaced by AC impedance that takes both contributions into account. Results may be depicted in Cole–Cole plots [23, 91, 92] of the impedance or in plots of the two components of the dielectric constant as a function of frequency [28]. The methods are still under development and refinement, especially with the goals of miniaturization and of enhanced resolution, but can now be considered as established [8, 51, 70, 109].

11.2 Theoretical Background of Bioimpedance Spectroscopy

11.2.1 General Considerations

Isolated charges are rare in nature under equilibrium conditions: each charge usually has a countercharge close by so that matter seen from the outside is essentially

electrically neutral. Only within small volumes, differences in electronegativity lead to local charge inhomogeneities as for example the formation of ions upon the dissolution of salts in aqueous solution or the formation of polar regions in molecules (partial charges).

Charges are the sources of fields. Their separation results in electric field gradients, and thus in differences of electric potential. Negative charges will be drawn to higher potential, and positive ones to lower potential. This is the origin of electric currents, and of the formation of shells of counter-ions around dissolved ions of opposite charge.

It will be shown that in principle all these phenomena may be integrated into the concept of dipoles (or multipoles). The ionic currents in electrolyte solutions are in a sense always dual currents where an electric potential difference $\Delta\Phi$ causes a motion of cations in one direction and a related flow of anions in the opposite direction. The fractional respective contributions to the total current are described by ionic transfer numbers, and the solution is polarized as long as the field is applied. The total current i follows Ohm's law:

$$\begin{aligned} i &= \frac{\Delta\Phi}{R} = \Delta\Phi \cdot G \\ &= \Delta\Phi \cdot \sigma \cdot g \end{aligned} \tag{11.1}$$

where R is the resistance and its inverse G the conductance.

The conductance can be broken down to a material-specific conductivity σ and a geometrical factor g (usually $g = \frac{A}{l}$, for the case of a current between two parallel metallic plates of area A and distance l that are connected to a power supply).

However, with increasing frequency ions become restricted to move due to inertia but rather respond to the potential by re-orientation of their dipole moments: the ionic conductivity σ drops from the steady state value σ_0. In this case (details see below), the system is better described by the complex dielectric constant

$$\varepsilon = \varepsilon' + \imath\,\varepsilon'' \tag{11.2}$$

11.2.2 Dipoles and Polarization

Dipoles are abundant in nature: they appear as soon as the centres of negative and positive charge distributions do not coincide. Their strength is described by the dipole moment $\underline{\mu}$ (the vector character of the dipole moment is abandoned here and μ is adopted for ease of discussion as scalar dipole moment). Upon bond formation among atomic partners of very different electronegativities, molecules with permanent dipole moments are formed [28]. The most prominent example is water [22] (see Fig. 11.1), not only because of its large quantity but also because of its role as a solvent for many chemical reactions and especially its role in biosystems [7, 22, 58, 97, 100, 114, 121]. External electric fields may enhance permanent dipole moments [99, 117, 123, 129], and initially nonpolar material may acquire an induced non-permanent dipole moment [10, 73, 116, 117].

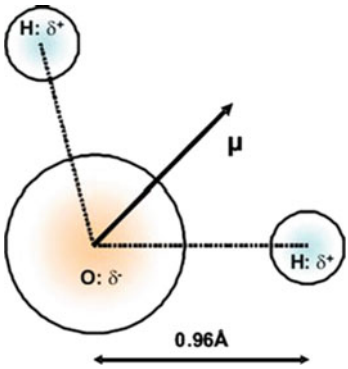

Fig. 11.1 Schematics of water molecule H_2O as an example for molecular dipole due to partial charges δ^+ and δ^-. Dipole moment: μ=1.85 D, angle suspended between oxygen–hydrogen bonds: 104.5°.

Dipoles interact with each other. Molecules with permanent molecular dipole moments tend to align and to develop ordered structures with a spontaneous macroscopic polarization $\underline{P} = \sum_i \underline{\mu}_i$ as in liquid crystals [25]. The dipole characteristic of fluctuating electron density even gives rise to the van der Waals interaction [83]. The degree of structure formation is hampered by temperature as thermal energy induces fluctuations into the system of interacting dipoles and thus prevents the formation of perfect dipole crystals at all realistic temperatures. As a result, the spontaneous polarization obtained from dipole interactions is permanent only below a sufficiently low temperature (called Curie temperature) and then the material is ferroelectric [5, 6, 54, 60, 81, 99].

Still, some local order may spontaneously arise due to dipole interactions, for example along charged interfaces. This is the case when electrodes are in contact with electrolyte solutions. Here, an electrochemical reaction with electron charge transfer results in the built up of an interfacial Nernst potential [41] (see also Galvani potential). A different case is the interface between cell surfaces (biomembranes) and adjacent liquid. Most cell membranes carry a net negative surface charge as there are only neutral or negatively charged lipids in nature. Moreover, most proteins are as well slightly negatively charged under physiological conditions (pH$\sim$7.4). Therefore, biointerfaces are typically negatively charged and exhibit a surface electric potential Φ_{surface} that exponentially decays into the equilibrium potential of the bulk liquid with a characteristic constant λ_D, the Debye length

$$\Phi_{\text{surface}}(x) = \Phi_0 \cdot e^{-\lambda_D x} \tag{11.3}$$

where x signifies the distance from the cell surface with potential Φ_0. If the cell was not immersed in electrolyte solution, the surface potential would decay infinitely slowly. The presence of charges and polarizable components in the electrolyte solutions around a charged surface (ions, cell membranes, electrodes, etc.) causes a faster decay of the electric potential. This is evident in a smaller Debye length – the surface charge is said to be screened.

The value of the Debye length λ_D depends on the ionic strength I of the electrolyte solution around the biological cell or tissue, the dielectric constant ϵ' of the solution and the temperature T so that for dilute salt solutions and in the limits of the Debye–Hückel theory [51, 97],

$$\lambda_D = \sqrt{\frac{\varepsilon_0 \varepsilon' \cdot kT}{2N_A e_0^2 \cdot I}} \tag{11.4}$$

with $I = \frac{1}{2} \sum_i c_i z_i^2$ for the ionic strength.

c_i and z_i are the molar concentration and charge number, respectively, of the i^{th} type of ions in the electrolyte solution; ε_0 the vacuum electric permittivity; N_A the Avogadro constant; e_0 the elementary charge and k the Boltzmann constant. All ions present in the electrolyte solution contribute to the value of I. For example, Eq. (11.4) yields values of $\lambda_D \approx 1$ nm for 100 mmol NaCl but $\lambda_D \approx 0.6$ nm for 100 mmol $CaCl_2$, because of the higher ionic strength due to the divalent Ca^{2+}, and $\lambda_D \approx 0.8$ nm for 140 mmol NaCl (∼physiological osmolarity). Equation (11.4) is an approximation for dilute ionic solutions and it will, for many ions, fail in the range of physiologically relevant concentrations. In that case, either semi-empirical corrections must be applied or the effective values of λ_D must be determined experimentally by measuring the zeta potential for ion concentrations above 100 mmol [51].

11.2.3 Electric Dipole Layers

Following the Gouy–Chapman theory, the reason for the decay of the surface potential is the formation of interfacial dipolar layers whenever the interface is immersed in electrolyte solution (see Fig. 11.2). In biological systems, the dipoles of the solvent water will wet the polar interface by orienting themselves appropriately: the end of the water dipole with the positive partial charge will on average be closer to a negatively charged interface than the opposite end. A first hydration layer forms. At the same time, the layer potential will decrease proportionally to $\sqrt{\varepsilon'}$, where ε' is the zero frequency real part of the dielectric constant of water (∼ 81). ε' is also called electric permittivity.

Through the first hydration layer a dielectric polarization is generated that decreases the electric field in the solvent as compared to the value it would have had without the dielectric polarization. The next water layer has the same orientation but is less ordered due to the higher distance from the charged interface. Proceeding further towards the bulk water phase, the orientation of the dipoles gets more and more diffuse until finally no net polarization persists and the water dipoles are uniformly oriented on average: this condition is reached for $\lambda_D x \cong 8$.

In electrolyte solutions when there are ions dissolved in water, each ion carries its own hydration shell (see Fig. 11.2) and can be envisaged as a dissolved dipole by its own. Thus, another type of polarization will additionally be caused by a redistribution of the ions along polar interfaces, causing the formation of Stern

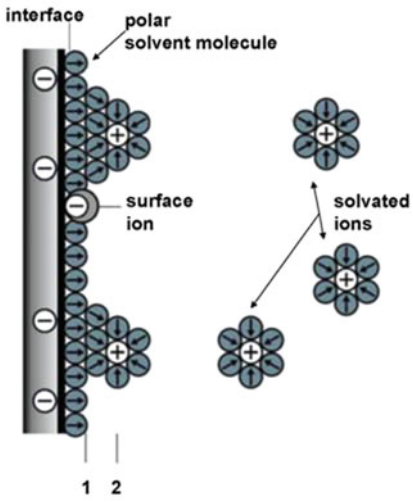

Fig. 11.2 Formation of interfacial layers. Solvent shells of decaying polarization due to negative interfacial charges. Accumulation of positively charged ions in layers close to the interface. Bulk ions in hydration shell. 1, inner Helmholtz layer; 2, outer Helmholtz layer.

and Helmholtz layers [12, 19, 69, 93, 97, 100, 138]. In the example of Fig. 11.2, positively charged ions are preferentially dragged towards the negatively charged interface whereas their negatively charged counter-ions are repelled. Thus, ionic double layers are formed (Helmholtz layers), again with decreasing order as the distance from the interface increases. It might even occur that ions partially slip off their hydration shell and get specifically adsorbed to form a well-defined Stern layer (not shown here). The potential drops exponentially, its course being determined by the Debye length λ_D as approximated by Eq. (11.4), depending both on the ionic strength due to the electrolyte and on the dielectric constant of the solvent. Again, thermally induced fluctuations counteract the formation of such meta-stable dipole-driven structures and the layers become increasingly diffuse with increasing distance from the polarizing interface. Finally, at sufficient distance, the interfacial charge is totally screened and the electrolyte solution becomes a homogeneous liquid of uniformly distributed dissolved ions.

11.2.4 Effect of External Fields

11.2.4.1 Motion in External Fields

External electric fields may be applied to any kind of sample by firmly contacting metallic electrodes to it (see Fig. 11.3, to be discussed further later on) and then connecting the electrodes to a power supply. The presence of the external field will influence and enhance the formation of dipoles, and will induce a macroscopic polarization (see below). The electric forces on charges may cause electro-migration or electro-rotation [39, 47, 107]. Electro-migration may be used to position and guide colloidal particles, like small drug crystals, vesicles or whole cells [124].

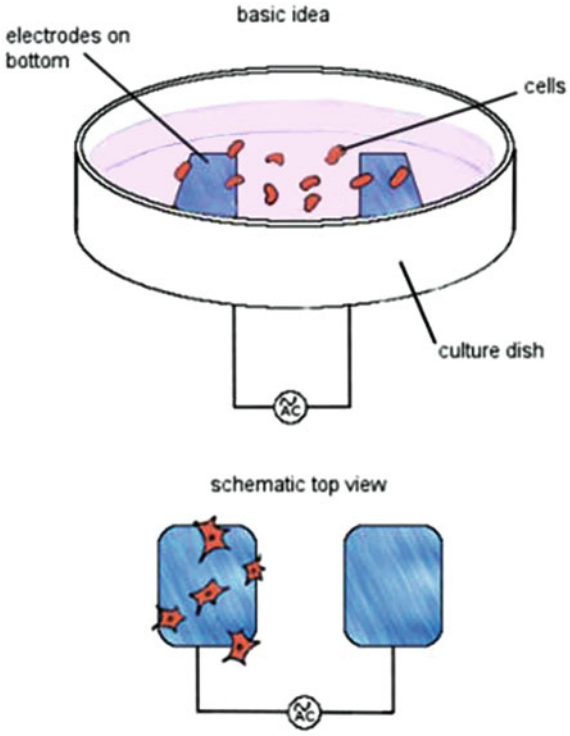

Fig. 11.3 Sketch of set-up for performing impedance measurements on a cell culture under the fluorescence microscope. Cells are grown on an agar gel in a Petri dish in proper buffer conditions. Metallic electrodes are attached to the bottom of the dish and attached to an AC power supply and serve to apply various types of electric fields. The top view exhibits that some cells migrated to one of the electrodes under the influence of an applied field and firmly attached to it.

Alternatively, in electrophoresis, it may serve for analytical purposes, making use of the electrophoretic mobility u of charged particles

$$u = \frac{v}{E} \tag{11.5}$$

where

$$E = \frac{\Delta\Phi_{\text{applied}}}{d} \tag{11.6}$$

is the electric field due to the applied external potential difference (voltage) $\Delta\Phi_{\text{applied}}$ between the electrodes of spacing d, and v is the so-called drift speed of the colloidal particles. The drift speed may be observed directly when watching the motion of the particles via optical microscopy. It depends on the effective charge of the moving particle ($z_i \cdot e_0$) as well as on the friction the object experiences when moving in its surroundings

$$u = \frac{z_i \cdot e_0}{6\pi \cdot \eta \cdot r}. \tag{11.7}$$

Here, η is the local viscosity which the mobile particle of radius r experiences from its surrounding medium (usually, the buffer). However, such a simplified system is not realistic since the particle carries its double layer (Fig. 11.2). In a more precise approach, one has to consider the surface charge of the particle with the resulting polarization of the adjacent Helmholtz layers and the contribution of the diffuse layer to the viscosity. Two extreme cases can be distinguished here, namely the one where the particle is small compared to its Debye length ($\lambda_D \cdot r = 1$, small particle with relatively thick double layer) and the other one, where a very big particle is surrounded by a relatively thin double layer ($\lambda_D r \to \infty$). Both are described by the theory of Hückel and Smoluchowski, respectively:

$$u = \frac{2\varepsilon_0 \varepsilon' \zeta}{3\eta} \text{ for } \lambda_D \cdot r = 1 \tag{11.8}$$

$$u = \frac{\varepsilon_0 \varepsilon' \zeta}{\eta} \text{ for } \lambda_D \cdot r \to \infty \tag{11.9}$$

The term ζ in these equations is the so-called zeta potential [83, 91, 93] that signifies the value of the surface potential at the location of the slipping plane that separates the surface-bound fluid (Helmholtz layers) and the freely mobile bulk fluid. The value and position of ζ can be determined experimentally.

11.2.4.2 Polarization in Electric Fields

External fields will apply forces to charged particles and dipoles, and they induce dipole moments to initially nonpolar systems and as well enhance initial dipole moments. As another effect, external fields may partially compensate the disturbing effect of thermal fluctuations. Therefore, the dipole–dipole interactions are strengthened compared to the situation where the external field is zero.

The external electric field will introduce a preferred direction into a system. It will apply an external force to the dipole moments. Thus, it will re-orient all dipole moments towards its direction if the viscosity is low enough, and it will stabilize the orientation of dipole moments in the direction of the field against thermal fluctuations. As a response to the external field, an additional polarization is induced into the dipole system that may overcome the spontaneous one by far. The dependency of the polarization on a steady applied field (DC field) is described by the Langevin–Debye function that accounts for the interplay of thermal disturbance (entropy) and electric organization (enthalpy).

11.2.4.3 Oscillating (AC) Fields

In general, the field must not be constant but may oscillate with a frequency f. The response of a system then depends on the system dynamics because the different possible processes are not equally compatible with the exciting frequency. The general course of the dielectric spectrum is schematically shown in Fig. 11.4.

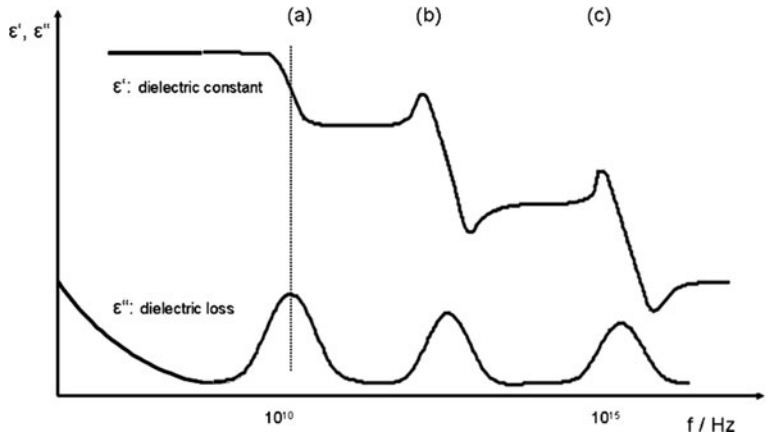

Fig. 11.4 Principal course of dielectric spectra, consisting of dispersion (ε') and absorption (ε'') loss spectrum. (**a**) dipole relaxations, (**b**) atomic vibrations and (**c**) electronic transitions. Each individual process contributes by a step to the total course of the dielectric spectrum. The initial decay on the very low-frequency slope of ε'' arises from conductivity contributions. The initial constant contribution in ε' is the steady-state dielectric constant.

11.2.5 Dielectric Spectrum

The dielectric spectrum, as schematically shown in Fig. 11.4, exhibits two curves, namely the dispersion curve $\varepsilon'(f)$ and the loss/absorption curve $\varepsilon''(f)$. Depending on the frequency range, two characteristic courses of the curves can be distinguished, attributed to relaxation (a) and to resonance processes ((b) and (c)). Of course, each system exhibits a whole series of these transitions.

The resonances are observed in the frequency range above 1 GHz ((b) and (c)) and occur when quantum mechanical processes take place: the (b) region is typical for transitions in molecular excitations (rotations, vibrations) and the (c) region accounts for the electronic transitions. Typical for resonance processes, the loss curve shows absorption peaks of Lorentzian shape with a natural line width Δf_{L} (width of the line at half maximum intensity) and an ideal decay/transition lifetime $\tau_{L0} = \frac{\Delta f_L}{2\pi}$ at low temperature and dilution. This ideal condition is almost never met as the excited particles cannot be prevented to exchange momentum when they bump into one another due to their thermal motion. This causes the so-called Doppler broadening of the natural line width such that $\tau_{\mathrm{LD}} > \tau_{\mathrm{L0}}$. The absorption peak is still very sharp, and its shape is still of Lorentzian type. The related dispersion curve exhibits abnormal dispersion with a negative slope in the region of an absorption peak and, in between two different resonance peaks, normal dispersion is found as it is known from optics, with the refractive index n ($n = \sqrt{\varepsilon_0 \varepsilon'}$) increasing with frequency.

The course of the dispersion and loss curves is totally different in the low-frequency range (a): first, the absorption peaks are much broader compared to the

resonance peaks, exhibiting a Debyean shape. The dispersion curves start with a constant value of ε' followed by a smooth continuous drop $\Delta\varepsilon_j'$ for each distinct relaxation event that takes place (see Fig. 11.16). This part of the dielectric spectrum is the range of the dipole relaxations.

11.2.5.1 Properties of the Dipole Relaxation Spectrum

Dipole relaxations occur in the frequency range Hz to GHz. They are characterized by a typical course of dispersion ($\varepsilon'(\omega)$) and absorption ($\varepsilon''(\omega)$) curves that are connected by the Kramers–Kronig relations [48, 64, 65, 68]. The course of $\varepsilon'(f)$ and $\varepsilon''(f)$ was first described by Debye [28] as

$$\varepsilon'(f) = \varepsilon_\infty + \sum_j \Delta\varepsilon_j \frac{1}{1 + (f/f_j)^2} \quad \text{(dispersion, permittivity)} \tag{11.10}$$

$$\varepsilon''(f) = \Delta\varepsilon_j \frac{(f/f_j)}{1 + (f/f_j)^2} \quad \text{(absorption, loss).} \tag{11.11}$$

Here, f is the frequency of the exciting field (electromagnetic wave) and f_j the relaxation frequency of the jth dipole system. Each type of dipole (dipole system) contributes to a drop $\Delta\varepsilon_j'$ to the decay of ε' until the final value ε_∞ at infinitely high frequencies (optical range) is assumed.

In the purely Debyean case, the course of ε' and ε'' is symmetric on $\ln(f)$ and the peak maximum of the loss curve (ε'') is found at a frequency where the dispersion curve (ε') exhibits a turning point (see Fig. 11.4). Dielectric relaxation processes can be modelled by a harmonic oscillator that is excited by the electric force of the field on the dipole moments, resulting in a characteristic response eigenfrequency for each type of responding dipole system. This frequency is called relaxation frequency f_0, and it corresponds to a relaxation time τ_0. The relaxation frequency is characteristic for the dipole system (e.g. the dipoles of bulk water) and coupled to the relaxation time by

$$f_j = 2\pi\omega_j = \frac{2\pi}{\tau_j} \tag{11.12}$$

At zero frequency (constant field), the system is characterized by its resistance R and its electrical capacitance C. $C = \varepsilon_0 \cdot \varepsilon'(f = 0) \cdot g$ is determined by the zero frequency dielectric constant $\varepsilon'(0)$ that describes the steady polarization obtained in a material filled capacitor with the according dielectric properties. g is a geometric factor, which in case of a parallel plate capacitor is $g = \frac{A}{d}$ with d being the distance between two metallic plates of area A. The dipoles present will acquire a constant polarization $P = \varepsilon_0\varepsilon' E$. The presence of mobile charge carriers like ions in water will lead to a current $i = \frac{\Delta\Phi}{R} = \text{const}$ with an Ohm-type resistance R.

In the case of ions, R is given by the respective ionic conductivities following, e.g., the Debye–Hückel theory [97]. The presence of the direct current appears in the dielectric spectrum at the very low end with a decaying wing in ε''. Apart from the

switching-on and switching-off processes, a steady situation with constant current and polarization develops.

As soon as time-dependent fields are applied, the situation changes: as discussed above, the response obtained now depends on the system dynamics. Most evident, the mobility of the ions is limited. Therefore, the direct current decreases to zero as frequency increases (see Fig. 11.4) – the hydrated ions can no longer move in the field. Still, dipole polarizations will occur up to the GHz range when the relaxation of liquid water (~19 GHz) sets the end of dipole relaxations (all other dipoles in electrolyte solutions are less mobile) and the spectrum continues with the resonances. This is first realized in the context of the switching-on and switching-off processes when both the current and the polarization response are observed to be delayed with respect to the field:

$$P(t) = P_{\max} \cdot e^{-\tau t} \text{ (switching-on process)} \tag{11.13}$$

$$P(t) = P_{\max} \cdot (1 - e^{-\tau t}) \quad \text{switching-off process} \tag{11.14}$$

In such a so-called time-domain experiment, the measured time course can be disintegrated into contributions of j characteristic exponential rates of typical relaxation times τ_j such that

$$P(t) = P_{\max} \cdot \sum_j e^{-\tau_j t} \text{ (switching-on process)} \tag{11.15}$$

$$P(t) = P_{\max} \cdot \left(1 - \sum_j e^{-\tau_j t}\right) \text{ (switching-off process)} \tag{11.16}$$

Each characteristic rate obtained signifies system properties that depend on the interaction between specific dipoles, the temperature and the viscous properties of the dipole surroundings.

11.3 Experimental Set-up

Since the times of Debye, the investigation of the frequency-dependent response of dipole systems became the basis of the emanating techniques of dielectric spectroscopy or electrochemical impedance spectroscopy [12, 19, 52, 58, 69, 85, 93, 96, 104, 109, 110, 112, 114, 118–120, 138]. The names essentially result from the different application communities: dielectric spectroscopy focuses on the spectroscopic aspect that considers the dipole relaxations as a peculiar part within the total dielectric spectrum (this starts with the classical dipole relaxations and continues into the resonance spectra of the high-frequency regions that are dominated by quantum mechanical effects). The term impedance spectroscopy on the other hand emphasizes the aspect of measurement and engineering, interpreting the relaxations as contributions to the complex electrical resistance (impedance), observed in

a system responding to the excitation of an external field from the mHz to the GHz radiofrequency range [111].

Equations (11.13), (11.14), (11.15), and (11.16) represent prescriptions to perform dielectric spectroscopy by measuring the build-up or decay of polarization as a function of time after an instantaneous change of the electric field (electric step function). Such experiments are called time-domain spectroscopy. The alternative are the so-called frequency-domain experiments that are based on measuring the response of a system as it is excited by an oscillating field of frequency f and subsequently scanning the frequency stepwise in the (whole) dipole relaxation range 0 Hz to GHz. The different options are shown in Fig. 11.5. The results obtained from either method are equivalent and may be interconverted by Fourier transformation.

The total macroscopic polarization of the system can be measured by electrode set-ups that compare the amplitudes and phase shifts of a transient or reflected wave with the initial field applied or by impedance set-ups that determine the value and phase shift of an electric current upon an applied voltage [8]. Both methods are equivalent and yield the field response that can be described by the complex dielectric constant $\varepsilon = \varepsilon'(\omega) + \iota\varepsilon''(\omega)$, with an absorption term ε'' and a dispersion term ε'.

In terms of electrical components, this time-dependent behaviour can be described by complex impedances Z_j as a combination of resistances R_j and

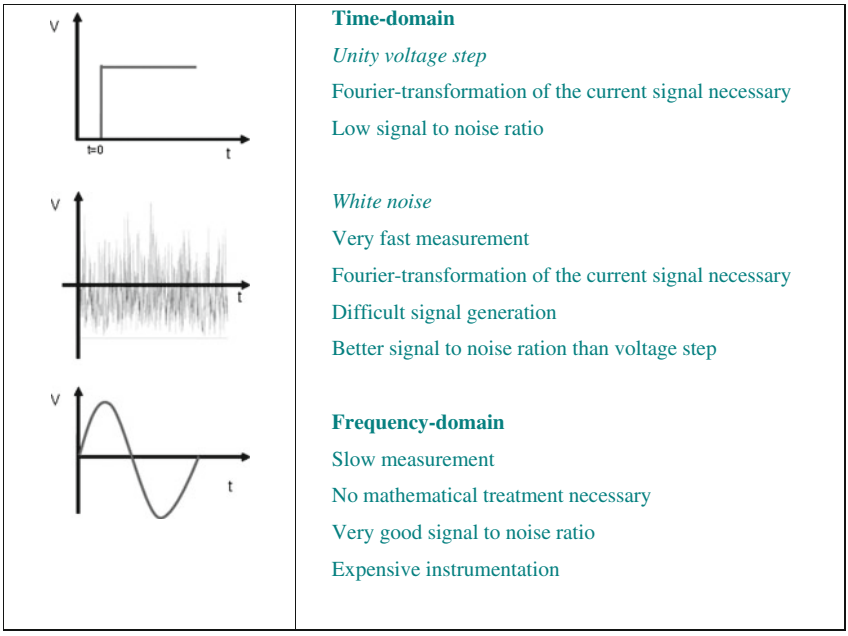

Fig. 11.5 Principal options for conducting frequency- or time-domain dielectric experiments. Excitation voltage as a function of time is either a step-function or a sinoidal wave. In the latter case, the acquisition of the full spectrum requires scanning all possible frequencies.

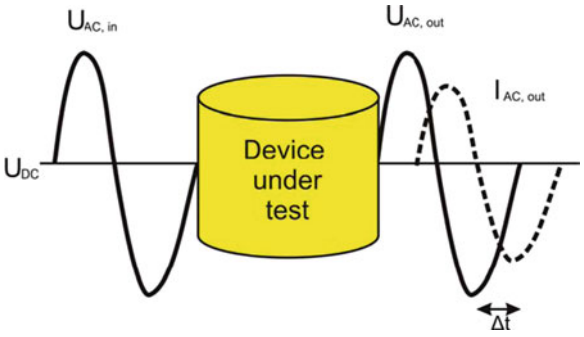

Fig. 11.6 Scheme of set-up for impedance spectroscopy

capacitors C_j. The principal set-up for such an experiment is sketched in Fig. 11.6.

An incident wave $U_{j\,\mathrm{AC,in}} = U_0 \cdot e^{\iota(\omega t+\varphi_I)}$ with an amplitude U_0, angular frequency ω and phase φ_U is applied to a sample. The outgoing wave $U_{j\,\mathrm{AC,out}}$ and the measured current $I_{j\,\mathrm{AC,out}} = I_0 \cdot e^{\iota(\omega t+\varphi_I)}$ are phase shifted by $\Delta\varphi{=}\varphi_U{-}\varphi_I$ as observed in a delay time Δt.

The complex impedance is then defined as

$$Z_i = \frac{U_{i\mathrm{AC,out}}}{I_{i\mathrm{AC,in}}} \tag{11.17}$$

and consists of a real part called resistance (coinciding with the value of R found under steady-state DC conditions) and an imaginary part called reactance.

The reactance accounts for the build-up of internal fields due to the exciting wave, in our case the polarization P as a response to the exciting field E. This term is responsible for the overall delay/phase shift.

The impedance Z is given as

$$Z = Z_R + Z_C = R - \iota\frac{1}{\omega C} \tag{11.18}$$

where Z_R and $Z_C = \frac{1}{\iota\omega C}$ are the resistance and reactance parts, respectively, of the impedance,

with

$$|Z| = \sqrt{R^2 + \left(\frac{1}{\omega C}\right)^2} \tag{11.19}$$

and

$$\Delta\varphi = \arctan\left(\frac{1}{\omega CR}\right). \tag{11.20}$$

11.4 Applications

There are many and very diverse applications of dielectric relaxation/impedance spectroscopy. The option of distinguishing between free and bound water makes these methods attractive to investigate corrosion [18, 133], changes in hydration in nanoporous systems [1] or transitions of thermo-responsive polymers [63, 118]. Dipole responses in biomaterials include studies covering a broad range of applications [62, 89, 119] from molecules [11, 34, 59, 130] via cells [84, 101, 103, 132] to tissues [27, 104]. In the framework of this book, two examples for application from the biosciences are being presented, both acquired in AC fields. The first one exemplifies the use of dielectric spectroscopy to identify and investigate specific dipole systems. The second one involves a miniaturized system developed for the purpose of biosensing.

11.4.1 Application to Colloidal Model Systems – Lipid Vesicles

Lipid membranes are frequently used as a biomimetic model scheme to investigate, in a controlled reduced system, basic properties and processes of biomaterial. In Fig. 11.7, a complete dielectric relaxation spectrum from a system of fully hydrated membranes of DMPC at ~308 K is shown, acquired with a coaxial probe that is connected to a network analyser [58]. Detailed analysis [13, 38, 58] exhibited two independently responding dipole systems that could be attributed to the polar headgroups of the lipids including their first tightly bound hydration shell of water and, as a second system, to a sequence of hydration layers. The headgroup system is relaxing with a pure Debyean characteristic, signified by a relaxation frequency $f_1 = 41$ MHz, whereas the hydration shell behaviour is best described by an exponentially decaying distribution of relaxation times, centred around 345 MHz and well below the value of 19 GHz for bulk water.

From the temperature course as depicted in an Arrhenius diagram (see Fig. 11.8), typical activation energies were determined for the two relaxation processes, namely 42 kJ/mol for the phosphatidylcholine headgroups connected to the myristoyl chains of DMPC, and 32 kJ/mol for the relaxation of the bound water. Most remarkably, a small jump in the relaxation frequency of the headgroups at ~297 K indicates the gel/liquid main phase transition of DMPC. This results in a sudden reduction of chain packing with a related release of headgroup dipole mobility.

Such an appearance is absent in a system like DOPC (T_m <273 K). Moreover, the presence of the kink in the oleoyl chain results in a lower chain packing and a related increase in the freedom of rotation for the attached choline group, which is evident in a reduced activation energy of 34 kJ/mol. Of course, the headgroup relaxation frequency is unchanged and likewise the hydration water along a DOPC interface exhibits essentially the same activation energy (31 kJ/mol) as measured for a DMPC interface.

Evidently, the dielectric spectrum allows tracing changes in molecular packing within the lipid membrane. Thus, it is a promising tool to monitor adhesions and insertions of, for example, drug molecules. One of the most obvious applications

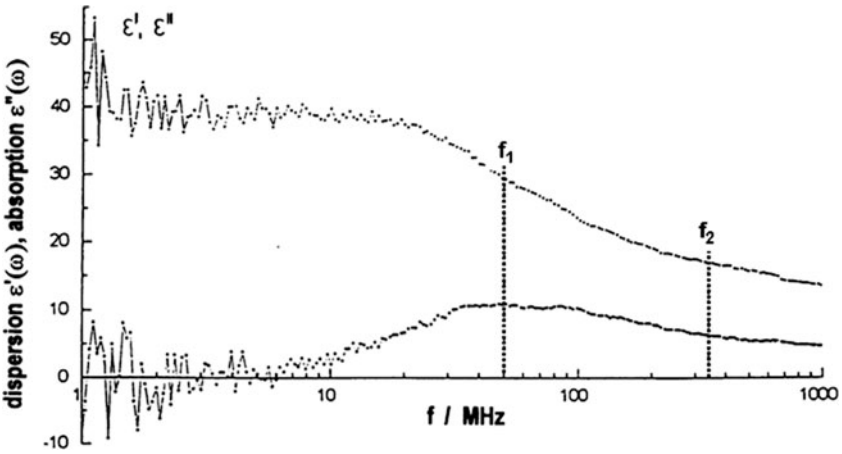

Fig. 11.7 Frequency-domain dielectric spectrum acquired on a system of lipid vesicles (DMPC). Analysis revealed two overlapping dipole resonances signified by the frequencies f_1 and f_2.

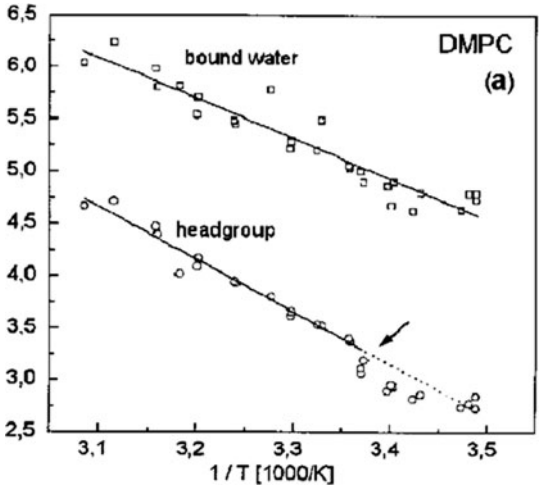

Fig. 11.8 Separate Arrhenius plots of the relaxation frequencies from the two dipole systems of lipid headgroups (phosphatidylcholine) and interfacial water (hydration shells). Note the mobility jump upon phase transition at ~23°C.

is the investigation of the state of interfacial water. Here, the dielectric spectra give insight into modifications in hydration [63, 76, 100, 119], for example due to solutes that change the local water structure (as sugars do) or upon surface binding of macromolecules that will disturb the hydration shell.

11.4.2 Application to Living Biomaterial

11.4.2.1 Lab-on-a-Chip Systems in General

Impedance measurements can be used to monitor cell behaviour in vitro [101] and in vivo [4, 45, 131]. Recently developed chip-based methods allow for spatial and

temporal control of cell growth and cell stimuli. These approaches lead to new microsystems, which are multifunctional platforms and permit the monitoring of basic biological parameters. Besides that, they may as well serve as cell-based sensors with implemented biochemical, biomedical, biophysical and environmental functions. These microsystems may imply many steps from the preparation of a cell culture sample, subsequent specific treatment and cell selection and, finally, biochemical analysis [105]. Such cell-based biosensors can report the physiological changes of the cells during the culturing and during treatment including their proliferation activity and changes in morphology. The chip read-out can be done using optical methods, for instance via fluorescence markers or microspectroscopy, and via an electrical output by measuring changes in the impedance or electrical potential as mentioned above, or via a combination of both methods [36].

Lab-on-a-chip devices are used in a wide variety of fields. They are being continuously developed, taking up the new trends and methods from technological developments. With modern techniques such as AFM and advanced fluorescence methods (e.g. single-particle tracking [31]), it is now possible to study single molecules in conditions that resemble in vivo circumstances. Another famous example is the Patch-Clamp technology, developed by Sakmann and Neher that allows studying single-molecule ion channels in living cell membranes [104]. All these methods are in detail very tedious and therefore mainly used in the experimental research field. Still, they are the foundation of chip-based methods which in the future shall serve as manageable tools in the application lab. Complex devices are being engineered that process multiples of events and reactions in order to simultaneously acquire manifold information, not restricted to only one type of molecule or an isolated reaction.

At the same time, sample volumes are minimized and observation scales shall reach sizes for features below the micrometre range. Therefore, lithographic approaches for processing hard and soft materials are used and combined with microfluidics and biochemical patterning [24]. An example for this continuing integration and minimization process is the development of planar parallel Patch-Clamp devices that make it possible to run 48 Patch-Clamp recordings at a time [14, 36]. The pre-patterning of active biomaterial on surfaces, known from AFM and from studies with optical tweezers [49], is now also used to specifically deposit and orient cells with respect to single chip elements [24].

Another application of lab-on-a-chip systems is the scaling down of chemical and biochemical analytical reactions. This is very attractive since smaller volumes of reagents are needed. This is more cost effective, the product output is faster and the production process is more environmentally appealing [55]. Miniaturization already started in 1999 when Agilent launched their 2100 Electrophoresis Bioanalyzer. This system contains a microfluidic-based platform for the analysis of DNA, RNA, proteins and cells. In 30 min 16 samples of reverse transcriptase–polymerase chain reactions (RT-PCRs) could be processed, an analysis that takes many hours with traditional methods. In continuation of the technological evolution, digital array chips were developed that carry microfabricated compartments for 9000 PCRs at a time [72]. This is only possible by use of semiconductor fabrication techniques from interdisciplinary crossover and exchange of technologies. Nowadays, solid-phase

and combinatorial chemistry and molecular biology micro-arrays are created with millions of probes for DNA and RNA diagnostics [55]. As another step of integration, medical diagnostics made use of both systems, PCR and DNA micro-arrays, and combined them for the detection of viral and bacterial pathogens [21, 105]. However, this kind of medical diagnostics is not restricted to DNA and RNA detection. Other approaches are immunological techniques that can be combined with chip technologies to detect virus particles or protein variations caused by infections [21] in a fast and reliable way. The amount of potential applications seems unlimited.

In summary, lab-on-a-chip systems constitute a new generation of devices for miniaturization and integration of a complex set of functions. Combined with microfluidic systems, there is now the opportunity to develop new diagnostic systems for health care. Lab-on-a-chip systems have many advantages, such as being inexpensive, precise and reliable, and they can easily be adopted for the creation of portable point-of-care systems.

11.4.2.2 Impedance Spectroscopy with IDES in Lab-on-a-Chip Devices

As an example for an integrated lab-on-a-chip system, cell-based sensors using interdigitated electrode structures (IDES) for measurements of cell impedances with the goal of monitoring physiological changes are presented [56].

With the cell-chip technology two different subjects can be addressed. First, different influences on cells during their cultivation on chips, such as temperature, chemical compounds or nutrition factors, can be monitored; second, basic biological insights in the cell and tissue behaviours can be obtained. For the monitoring of cell proliferation and morphology, impedance measurements are a non-invasive tool which allows measurement of cell kinetics simultaneous to cultivation. Invasive procedures such as collecting cell samples or addition of chemicals, as commonly used in molecular testing approaches, are avoided [46].

The electric field of planar electrodes on a chip does not extend deeply into the volume of the working solution. Therefore, signal-to-noise ratio is best and analysis is easiest for samples that are confined closely to the electrodes or, optimally, tightly attached to the chip surface. In a non-chip conformation, parallel electrodes at short distance may serve to investigate cells suspended in the enclosed volume between the electrodes.

In Fig. 11.9 an example of an integrated chip for the monitoring of cell proliferation is shown. The chip contains sensor electrodes for impedance measurements and sensors for the measurement of the physiologically relevant parameters of pH, pO_2 and temperature. For a detailed description of the chip, please refer to Chapter 10 of this issue.

There are different protocols for impedance measurements. For example, the attaching and spreading of cells on a chip surface easily requires a period of hours or even days. In such a case, it is sufficient to restrict the impedance measurements to one defined test frequency. This optimal frequency differs among different cell types and needs to be determined ahead of the experiments using cells attached onto the chip surface [101]. The test frequency is then determined from the maximal

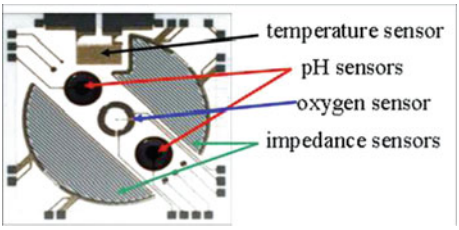

Fig. 11.9 Lab-on-a-chip device with integrated temperature, pH and oxygen sensors. For impedance measurements, IDES structures can be used (provided by cellasys GmbH, Munich, Germany).

Fig. 11.10 Principal set-up for the measurement of cell impedance of a confluent cell layer on a planar electrode structure

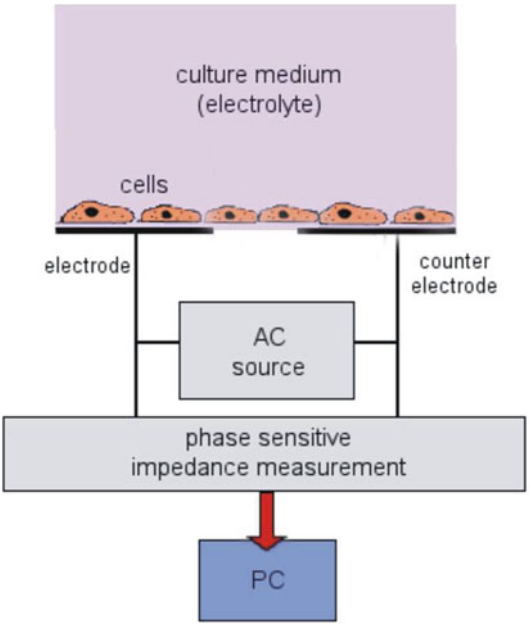

response obtained from full impedance spectra in the range of beta-dispersions (see Section 11.5).

There is non-linearity in the response of biological systems that requires the impedance measurements to be done at very low excitation amplitude with AC voltages in the order of ~10 mV_{pp} (pp: peak-to-peak). A general set-up for confluent cell layers is shown in Fig. 11.10.

A typical normalized impedance spectrum of attached cells and of cells after a Triton X-100 treatment is shown in Fig. 11.11. Healthy cells exhibit a characteristic course of the spectrum with a maximum at a specific frequency. Treatment of the cells with Triton X-100 leads to the destruction of the cell membranes and therefore to the detachment of the cells from the chip surface. As a consequence, the spectrum is modified: the signal amplitude around the initial maximum drops. Hence, the

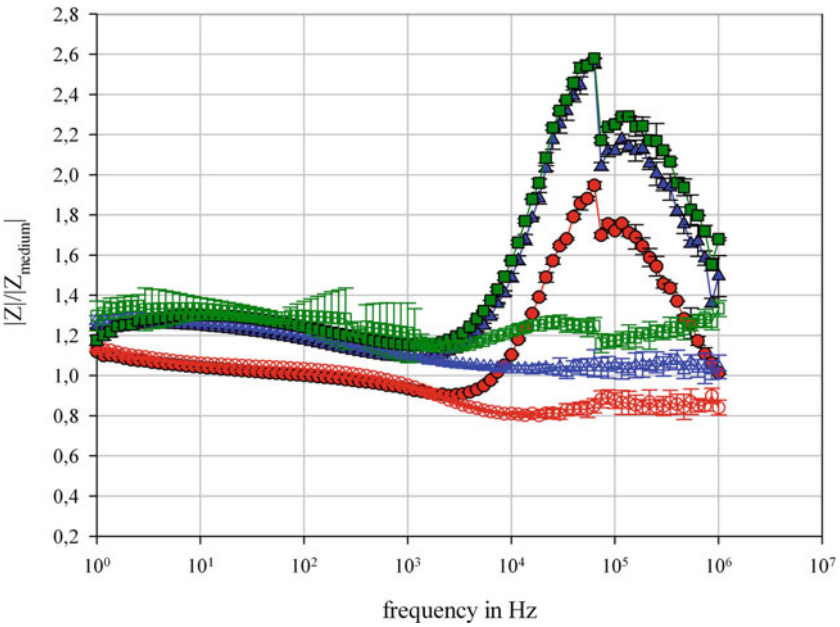

Fig. 11.11 Normalized impedance over frequency of three different chips with a confluent cell layer. Curves with full circles are impedance spectra of confluent cells before the treatment with 0.2% Triton X-100 (mean values). Curves with empty circle are impedance spectra of confluent cells after the treatment with 0.2% Triton X-100 (mean values). Data of the green, the blue and the red curves are obtained from the same chip, respectively. Error bars indicate the standard deviation.

system can be calibrated according to the change of signal amplitude at the specific test frequency to determine the mass of the adhered cells.

Further experiments can then be carried out using only this frequency, and the cell response towards different influences (e.g. chemical treatment and temperature) can be monitored over time. An example for an impedance measurement at this optimal test frequency is given in Fig. 11.12.

Figure 11.13 schematically shows the results from impedance measurements over time during the attachment of the cells onto the chip surface together with results from a measurement without any cells, both conducted at the same well-defined excitation frequency.

A model for the interpretation of such impedance measurements of cells on the surface of the chip, together with its electronic equivalent circuit diagram, is depicted in Fig. 11.14. The result from the experiments consists of a set of frequency-dependent complex impedances, given as imaginary and real parts of the impedance. These data can be entered into a Cole–Cole plot (see Fig. 11.15). Now, an attempt can be made to fit these data to a theoretical model. The physical parameters of the biological material under study can then be expressed as specific values in terms of resistances and capacitances that are entered into the fitting from

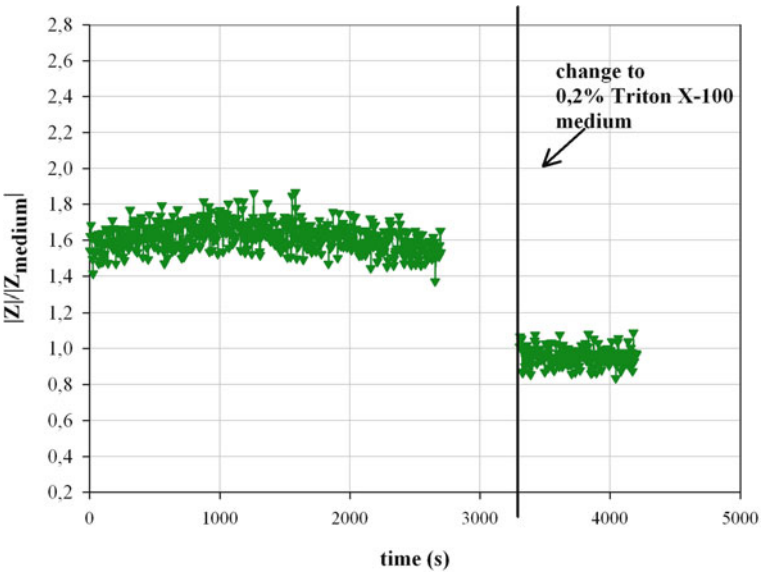

Fig. 11.12 Normalized values of the impedance of cells measured at their optimal test frequency over the time before and after the treatment with Triton X-100

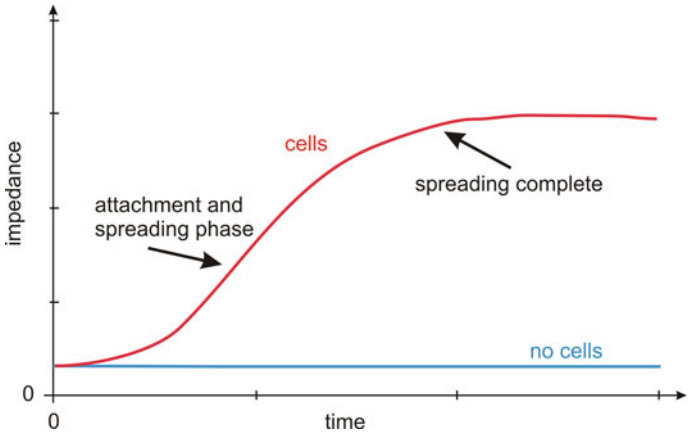

Fig. 11.13 Impedance measurement over the time during the attachment and spreading of cells on the chip surface (red curve) and without any cells (blue curve)

the model. Essentially, the parameters of an equivalent electrical circuit are fitted to the points of a measured impedance spectrum by means of complex least square fitting [8].

The basis of such a fit is derived from a properly chosen equivalent circuit like the one proposed in Fig. 11.14, right. It represents a simple model for the electrical current in a layer of biological cells on a chip. For the case given, it consists of

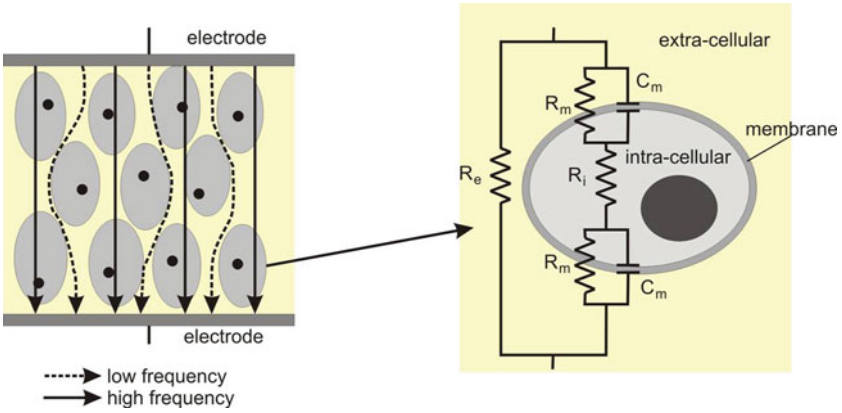

Fig. 11.14 Left: Current paths at high (full line) and low frequencies (dotted line) through a confluent cell culture on IDES. Right: equivalent electrical circuit of a cell.

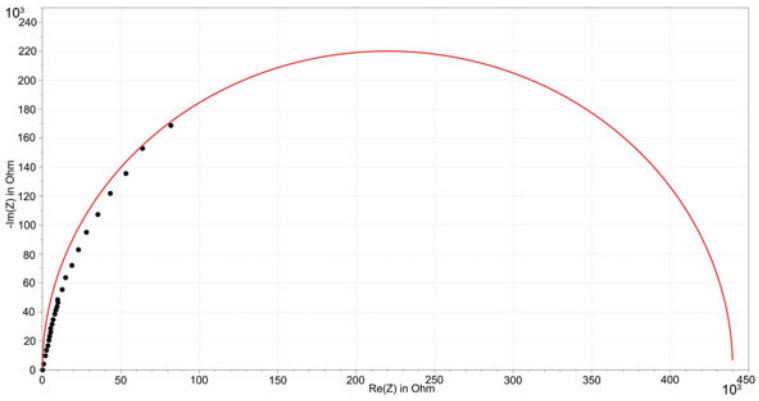

Fig. 11.15 Impedance spectra of a confluent cell layer (dots) and a fit on the equivalent circuit

two parallel current paths, one that runs exclusively through the extracellular liquid and a second current which flows through the cells. The extracellular liquid is represented by the resistance R_e, which is mainly dependent on the ionic composition of the fluid. In the case of tightly packed cells this current can be omitted. The second current is more complex and runs through the intracellular part of the cytosol represented by the resistance R_i and through a transmembrane part (two times, as the current crosses the cell membrane twice). In the model, this transmembrane part is entered as a parallel combination of a capacitor and a resistor. The capacitor is described by the capacitance of the cell membrane C_m, and the parallel resistor represents the membrane through which the leak current flows and is entered as a membrane resistance R_m [70]. On the left side in Fig. 11.14, a schematic top view

of the chip with the cultured cells is given. At low frequencies, the capacitor C_m acts like an open circuit and therefore most of the current flows through the pure Ohm part of the circuit, represented by R_e and R_m, R_i. R_m is in the range of MΩ and therefore exceeds typical values of R_e by far. Thus, the current flows mainly through the extracellular path (R_e) instead of through the cells. At high frequencies, the situation changes and the capacitor C_m acts like a short circuit. The alternating electric potential is transmitted via C_m into the intracellular volume and results in an intracellular current that is limited by R_i, in parallel to the leakage current across R_m. R_m contributes only a small portion and can be neglected in most cases. The total current is thus essentially composed of a transmembrane intracellular portion (C_m, R_i) and a parallel extracellular portion (R_e). The relative contributions depend on the packing density of the cells and on the composition of the intra- and extracellular ionic solutions.

The complex impedance for a resistor in parallel to a capacitor is given by

$$Z_{R||C} = \frac{R_m}{1 + \iota\omega R_m C_m} \tag{11.21}$$

Hence, the total complex impedance of the equivalent circuit shown in Fig. 11.14 is given by

$$Z_\iota = \frac{(2 \cdot Z_{R||C} + R_i)R_e}{R_e + R_i + 2 \cdot Z_{R||C}} \tag{11.22}$$

Complex Numbers

Complex numbers consist of two contributions, called the real and the imaginary parts. A complex number z may be written as

$z = x + \iota y$, where x signifies the real part and y the imaginary part of the number, and ι is the imaginary unit with $\iota^2 = -1$. The numerical value (or modulus) of z is given as $|z| = \sqrt{x^2 + y^2}$. Complex numbers are often geometrically represented in Argand diagrams which resemble 2D vector diagrams, where z is then found as a position vector of length r under an angle (or phase) φ, resulting from the vector sum of x and y. Accordingly, z can be written in polar form as $z = r \cdot e^{\iota\varphi}$, and $|z| = r$.

The complex conjugate of z is z^*, defined as $z^* = x - \iota y$, such that $z \cdot z^* = |z|^2$, or $|z| = |z^*|$. This allows to extract the imaginary and real parts from z by use of the complex conjugate:

$$\mathrm{Re}\,(z) = \frac{1}{2}\left(z + z^*\right) \quad \text{and Im}\,(z) = \frac{1}{2\iota}\left(z - z^*\right).$$

Added by the editors

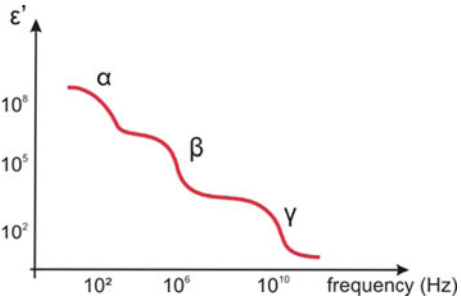

Fig. 11.16 Scheme of electric permittivity of biological materials (details see below). The α, β, γ drops with $\Delta\varepsilon'_j$ with $j = \alpha, \beta, \gamma$ account for typical relaxation processes relevant for biomaterial (details see text).

The impedance Z can be represented in a Cole–Cole plot [20, 23, 51, 91] that gives a semicircle plot in the complex space. Figure 11.15 shows a complex non-linear fit of a measured impedance spectrum of a confluent cell layer to the equivalent electric circuit shown in Fig. 11.14. The impedance spectrum was measured in a finite frequency range up to 100 kHz, and the simulation was performed between 0 Hz and 100 MHz.

11.5 Phenomenological Relaxation Regions in Biomaterial

Electrical bioimpedance spectroscopy addresses the measurement of the electrical impedance of a biological sample. It can reflect some interesting physiological conditions and events such as changes in mobility and hydration, or it can serve as a phenomenological fingerprint of a tissue/cell type to be distinguished from another species. It thus supplements other system information, as proliferation rate, gene expression, oxygen consumption or local pH value. The passive electrical properties of materials can be described by their dielectric constants ε_i as well as by their electric conductivity σ. For biological tissue and for cells those parameters depend dramatically on the frequency. This frequency dependence is noted as dispersions (Fig. 11.16). The origin of dispersion in biological materials is briefly discussed in the following [41, 46, 106, 108].

At low frequencies (<1 MHz) the conductivity of the tissue is determined by the conductivity of the electrolyte in the extracellular space. The total conductivity depends dramatically on the volume of the extracellular space. Some materials show dispersion (α-dispersion) with a middle frequency in the kHz range. It is assumed that interactions between counter-ions (ions bound at slightly charged surfaces) and biological membranes are responsible for this type of dispersion. Furthermore, it is believed that polarization of structures in the membranes (headgroup regions) is also involved in α-dispersion [58]. At frequencies below α-dispersion, the relative dielectric constant increases dramatically up to 10^7.

At radio frequencies (3 kHz–1 GHz), biological materials show the so-called β-dispersion with middle frequencies in the range of 100 kHz–10 MHz. The origin of this dispersion is the charging of intra- and extracellular ions and their interactions. At frequencies above β-dispersion, the impedance of the cell membranes can be neglected. An applied voltage causes a current which flows through the extracellular space as well as through the intracellular space/medium (Fig. 11.12, left). The β-dispersion can be superimposed by side dispersions caused by the relaxation of amino acids or by the charging of intracellular organelles.

At microwave frequencies (>1 GHz), biological materials show γ-dispersion which is mainly determined by the relaxation of water molecules in the material. Here, the presence of hydration shells can be detected, e.g. along lipid membranes [58]. The middle frequency is at 19 GHz, which is the relaxation frequency of free water. Frequency shifts can be caused by e.g. water-bounded proteins. Hydrated proteins show a large spectrum in the range from a few MHz to GHz that reflects the charged macro(ionic) molecule with its shells of bound water and electrolytes.

11.6 Conclusion

Dielectric relaxation spectroscopy (DRS)/electrochemical impedance spectroscopy (EIS) has turned out to be a powerful technique for studying dynamic properties in systems with polar components or reaction mechanisms in ionic solutions or at charged interfaces (electrodes, surfaces of cells, etc.). The beginnings of EIS can be traced to the work of Heaviside and Warburg, more than a century ago. Applications are as diverse as the investigation of corrosion processes (when the results of Epelboin and co-workers [18] in the 1960s propelled EIS into the forefront as a corrosion mechanism analytic tool [1, 74, 98, 133]), the properties of dissolved polymers [54, 62, 63, 78, 88, 118, 134, 136] and colloidal systems [9, 12, 17, 19, 29, 39, 53, 112, 115, 128]. The latter two topics directly connect to the biosciences as suspensions of isolated cells represent a special case of colloidal suspensions: accordingly, DRS and EIS are emanating techniques nowadays that are applied to colloidal systems including dissolved polymers [50, 51, 56, 62, 63, 87, 88, 89, 90, 135, 137] and cell suspensions [3, 20, 30, 39, 42, 43, 69, 75, 80, 86, 90, 94, 95, 103, 114], and even whole tissue [27, 79, 108, 137, 139]. A special and almost omnipresent case is the contribution of water that is found in hydration shells of dissolved ions [97, 100], polymers [59, 121, 126] and suspended colloids as cells [38, 40, 58, 59, 63, 76, 77, 80, 100, 121, 123, 129], behaving very different from the dielectric behaviour of bulk water [22, 77, 113]. Complex systems as an assembly of cells in a matrix of polymers and in aqueous electrolyte solution do however not obey the simple Debye law but require modifications that account for the geometry and related physical details of such distributed impedance systems [13, 17, 38, 52, 58, 66, 95, 96]. New technical developments as to the spectrometers [33], miniaturization of samples and probes [32, 61] and better mathematical modelling now

Abbreviations	Quantity	Unit, value
C_m	Membrane capacity	[F]; 1 F = 1 CV^{-1}
e_0	Elementary charge	1.602×10^{-19} C; C: Coulomb
ε_0	Vacuum electrical permittivity	$8.854 \times 10^{-12} \cdot C^2J{-}1^{m-1}$
ε'	Electric permittivity: real part of dielectric constant	
ε''	Imaginary part of dielectric constant	
f	Frequency; $\omega{=}2\pi f$	[Hz], Hertz
G	Conductance	$[\Omega^{-1}]$; $G = 1/R$
i	Electric current	
I	Ionic strength	[mol/l]
ι	Imaginary unit	
k	Boltzmann constant	$1.380{\times}10^{-23}$ JK^{-1}
λ_D	Debye length	[m]
μ, $\underline{\mu}$	Dipole moment	[D=Cm]; Debye
N_A	Avogadro constant	6.022×10^{23} mol^{-1}
Φ	Electrical potential	$[V{=}JC^{-1}]$
$\Delta\Phi$, (U)	Electrical potential difference, (voltage)	[V], Volt
φ	Phase (of a wave)	[°]
ω	Angular frequency	[Hz]
P	Electric polarization	[Cm]
R	Resistance	[Ω], Ohm
R_m	Membrane resistance	[Ω]
σ	Conductivity	$[\Omega^{-1}m^{-1}]$
T	Thermodynamic temperature [122]	[K], Kelvin
T_m	Melting temperature	[K], Kelvin
z	Ionic charge number	

AFM	Atomic force microscopy
DMPC	Di-myristoyl-phosphatidylcholine
DOPC	Di-oleoyl- phosphatidylcholine
DNA	Deoxyribonucleic acid
IDES	Interdigitated electrode structures
RT-PCR	Reverse transcriptase–polymerase chain reactions
PCR	Polymerase chain reaction
RNA	Ribonucleic acid

allow applying DRS and EIS to many systems and in advanced applications such as continuous process monitoring [32, 56, 57, 67, 119, 127, 134, 136] and medical diagnosis [27, 32, 35, 37, 71, 79, 84, 139] including non-invasive monitoring of glucose concentrations for diabetes patients [15, 16, 82, 125, 129, 130].

References

1. Alonso C, Andrade C, Keddam M, Novoa XR, Takenouti H (1998) Study of the dielectric characteristics of cement paste. In: Bonora PL, Deflorian F (eds) Electrochemical methods in corrosion research Vi, Pts 1 and 2, vol 289–282. Transtec Publications Ltd, Zurich-Uetikon, pp 15–27
2. Andersen SSL, Jackson AD, Heimburg T (2009) Towards a thermodynamic theory of nerve pulse propagation. Prog Neurobiol 88(2):104–113
3. Asami K, Sekine K (2007) Dielectric modelling of cell division for budding and fission yeast. J Phys D-Appl Phys 40(4):1128–1133
4. Awayda MS, Van Driessche W, Helman SI (1999) Frequency-dependent capacitance of the apical membrane of frog skin: dielectric relaxation processes. Biophys J 76(1 Pt 1): 219–232
5. Balke N, Bdikin I, Kalinin SV, Kholkin AL (2009) Electromechanical imaging and spectroscopy of ferroelectric and piezoelectric materials: state of the art and prospects for the future. J Am Ceram Soc 92(8):1629–1647
6. Bao DH (2008) Multilayered dielectric/ferroelectric thin films and superlattices! Curr Opin Solid State Mat Sci 12(3–4):55–61
7. Bao JZ, Swicord ML, Davis CC (1996) Microwave dielectric characterization of binary mixtures of water, methanol, and ethanol. J Chem Phys 104(12):4441–4450
8. Barsoukov E, Macdonald JR (eds) (2005) Impedance spectroscopy – theory, experiment and applications. Wiley, New York, NY
9. Blum G, Maier H, Sauer F, Schwan HP (1995) Dielectric-relaxation of colloidal particle suspensions at radio frequencies caused by surface conductance. J Phys Chem 99(2): 780–789
10. Bohmer R, Loidl A (1991) Dielectric investigations of pure and mixed fluorocarbons in their condensed phases. J Mol Liq 49:95–104
11. Bonincontro A, Risuleo G (2003) Dielectric spectroscopy as a probe for the investigation of conformational properties of proteins. Spectrochim Acta A Mol Biomol Spectrosc 59(12):2677–2684
12. Bradshaw-Hajek BH, Miklavcic SJ, White LR (2008) Frequency-dependent electrical conductivity of concentrated dispersions of spherical colloidal particles. Langmuir 24(9): 4512–4522
13. Brecht M, Klösgen B, Reichle C, Kramer KD (1999) Distribution functions in the description of relaxation phenomena. Mol Phys 96(2):149–160
14. Bruggemann A, Stoelzle S, George M, Behrends JC, Fertig N (2006) Microchip technology for automated and parallel patch-clamp recording. Small 2(7):840–846
15. Caduff A, Dewarrat F, Talary M, Stalder G, Heinemann L, Feldman Y (2006) Non-invasive glucose monitoring in patients with diabetes: a novel system based on impedance spectroscopy. Biosens Bioelectron 22(5):598–604
16. Caduff A, Talary MS, Mueller M, Dewarrat F, Klisic J, Donath M, et al. (2009) Non-invasive glucose monitoring in patients with Type 1 diabetes: a multisensor system combining sensors for dielectric and optical characterisation of skin. Biosens Bioelectron 24(9):2778–2784
17. Cametti C (2009) Dielectric and conductometric properties of highly heterogeneous colloidal systems. Riv Nuovo Cimento 32(5):185–260
18. Caprani A, Epelboin I, Morel P (1980) Potentiostatic investigation of the evolution of the cathodic current, near the corrosion potential, of a titanium rotating-disk electrode in aerated sulfuric-acid medium. J Less-Common Met 69(1):37–48
19. Chassagne C, Bedeaux D (2008) The dielectric response of a colloidal spheroid. J Colloid Interface Sci 326(1):240–253
20. Chelidze T (2002) Dielectric spectroscopy of blood. J Non-Cryst Solids, 305(1–3):285–294
21. Chin CD, Linder V, Sia SK (2007) Lab-on-a-chip devices for global health: past studies and future opportunities. Lab Chip 7(1):41–57

22. Clough SA, Beers Y, Klein GP, Rothman LS (1973) Dipole-moment of water from stark measurements of H2O, HDO, and D2O. J Chem Phys 59(5):2254–2259
23. Cole KS (1928) Electric impedance of suspensions of spheres. J Gen Physiol, 12(1):29–36
24. Craighead H (2006) Future lab-on-a-chip technologies for interrogating individual molecules. Nature 442(7101):387–393
25. de Gennes PG, Prost J (1993) The physics of liquid crystals, 2nd edn. Clarendon Press, Oxford
26. Deacon MP, McGurk S, Roberts CJ, Williams PM, Tendler SJB, Davies MC et al (2000) Atomic force microscopy of gastric mucin and chitosan mucoadhesive systems. Biochem J 348:557–563
27. Dean DA, Machado-Aranda D, Ramanathan T, Molina I, Sundararajan R, Ieee I (2006) Electrical properties of biological tissues – an impedance spectroscopy study. In 2006 Annual report conference on electrical insulation and dielectric phenomena, New York, NY, pp 357–360
28. Debye P (1929) Polare molekeln. Verlag Hirzel, Liepzig
29. Denton AR (2007) Electroneutrality and phase behavior of colloidal suspensions. Phys Rev E 76(5):051401-1–051401-11
30. Di Biasio A, Cametti C (2007) Dielectric properties of aqueous zwitterionic liposome suspensions. Bioelectrochemistry 70(2):328–334
31. Dietrich C, Yang B, Fujiwara T, Kusumi A, Jacobson K (2002) Relationship of lipid rafts to transient confinement zones detected by single particle tracking. Biophys J 82(1):274–284
32. Ding L, Du D, Zhang XJ, Ju HX (2008) Trends in cell-based electrochemical biosensors. Curr Med Chem 15(30):3160–3170
33. Doerner S, Schneider T, Hauptmann PR (2007) Wideband impedance spectrum analyzer for process automation applications. Rev Sci Instrum 78(10):9
34. Ebbinghaus S, Kim SJ, Heyden M, Yu X, Heugen U, Gruebele M et al (2007) An extended dynamical hydration shell around proteins. Proc Natl Acad Sci USA 104(52): 20749–20752
35. Edd JF, Horowitz L, Rubinsky B (2005) Temperature dependence of tissue impedivity in electrical impedance tomography of cryosurgery. IEEE Trans Biomed Eng 52(4):695–701
36. El-Ali J, Sorger PK, Jensen KF (2006) Cells on chips. Nature 442(7101):403–411
37. Fass L (2008) Imaging and cancer: a review. Mol Oncol 2(2):115–152
38. Feldman Y, Puzenko A, Ryabov Y (2002) Non-Debye dielectric relaxation in complex materials. Chem Phys 284(1–2):139–168
39. Foster KR, Sauer FA, Schwan HP (1992) Electrorotation and levitation of cells and colloidal particles. Biophys J 63(1):180–190
40. Foster KR, Schepps JL, Schwan HP (1981) Variation of dielectric-properties of tissues as a function of water-content. Studia Biophys 84(1):31–33
41. Foster KR, Schwan HP (1989) Dielectric-properties of tissues and biological-materials – a critical-review. Crit Rev Biomed Eng 17(1):25–104
42. Fricke H (1925) The electric capacity of suspensions with special reference to blood. J Gen Physiol 9(2):137–152
43. Fricke H (1953) Relation of the permittivity of biological cell suspensions to fractional cell volume. Nature 172(4381):731–732
44. Fukuda J, Khademhosseini A, Yeh J, Eng G, Cheng J, Farokhzad OC et al (2006) Micropatterned cell co-cultures using layer-by-layer deposition of extracellular matrix components. Biomaterials 27(8):1479–1486
45. Ghodgaonkar DK, Bin Daud A, Ieee I (2003) Calculation of Debye parameters of single Debye relaxation equation for human skin in vivo. In: 4th national conference on telecommunication technology, proceedings, Ieee, New York, NY, pp 71–74
46. Giaever I, Keese CR (1984) Monitoring fibroblast behavior in tissue culture with an applied electric field. Proc Natl Acad Sci USA 81(12):3761–3764

47. Gimsa J, Wachner D (1998) A unified resistor-capacitor model for impedance, dielectrophoresis, electrorotation, and induced transmembrane potential. Biophys J 75(2): 1107–1116
48. Gorter CJ, Kronig RDL (1936) On the theory of absorption and dispersion in paramagnetic and dielectric media. Physica 3:1009–1020
49. Gosse C, Croquette V (2002) Magnetic tweezers: micromanipulation and force measurement at the molecular level. Biophys J 82(6):3314–3329
50. Grant EH, Sheppard RJ, South GP (1978) Dielectric behaviour of biological molecules in solution. Clarendon Press, Oxford
51. Grimnes SJ, Martinsen OG (2008) Bioimpedance and bioelectricity. Academic, Oxford
52. Grosse C, Schwan HP (1992) Cellular membrane-potentials induced by alternating-fields. Biophys J 63(6):1632–1642
53. Grosse C, Tirado M, Pieper W, Pottel R (1998) Broad frequency range study of the dielectric properties of suspensions of colloidal polystyrene particles in aqueous electrolyte solutions. J Colloid Interface Sci 205(1):26–41
54. Horiuchi S, Tokura Y (2008) Organic ferroelectrics. Nat Mater 7(5):357–366
55. Janasek D, Franzke J, Manz A (2006) Scaling and the design of miniaturized chemical-analysis systems. Nature 442(7101):374–380
56. K'Owino IO, Sadik OA (2005) Impedance spectroscopy: a powerful tool for rapid biomolecular screening and cell culture monitoring. Electroanalysis 17(23):2101–2113
57. Kiviharju K, Salonen K, Moilanen U, Eerikainen T (2008) Biomass measurement online: the performance of in situ measurements and software sensors. J Ind Microbiol Biotechnol 35(7):657–665
58. Klösgen B, Reichle C, Kohlsmann S, Kramer KD (1996) Dielectric spectroscopy as a sensor of membrane headgroup mobility and hydration. Biophys J 71(6):3251–3260
59. Knab J, Chen JY, Markelz A (2006) Hydration dependence of conformational dielectric relaxation of lysozyme. Biophys J 90(7):2576–2581
60. Kochervinskii VV (2009) New electrostriction materials based on organic polymers: a review. Crystallogr Rep 54(7):1146–1171
61. Kohlsmann S, Hetscher M, Kramer K (1994) Application of a miniaturised probe for the acquisition of dielectric data in living systems. Z Naturforsch 49a:1165–1170
62. Korzhenko A, Tabellout M, Emery J (1999) Investigations of the biopolymers by dielectric relaxation spectroscopy. In: Wlochowicz A, TargoszWrona E (eds) Polymers and liquid crystals, vol 4017. Spie-Int Soc Optical Engineering, Bellingham, pp 68–73
63. Korzhenko AA, Tabellout M, Emery JR (2000) Dielectric relaxation properties of the polymer coating during its exposition to water. Mater Chem Phys 65(3):253–260
64. Kramers HA (1923) On the theory of X-ray absorption and of the continuous X-ray spectrum. Philos Mag 46(275):836–871
65. Kramers HA (1929) The dispersion and absorption of x-rays. Physikalische Zeitschrift 30:522–523
66. Krishna G, Schulte J, Cornell BA, Pace R, Wieczorek L, Osman PD (2001) Tethered bilayer membranes containing ionic reservoirs: the interfacial capacitance. Langmuir 17(16):4858–4866
67. Krommenhoek EE, Gardeniers JGE, Bomer JG, Van den Berg A, Li X, Ottens M, et al. (2006) Monitoring of yeast cell concentration using a micromachined impedance sensor. Sens Actuator B-Chem 115(1):384–389
68. Kronig RDL (1926) On the theory of dispersion of x-rays. J Opt Soc Am Rev Sci Instrum 12(6):547–557
69. Lisin R, Ginzburg BZ, Schlesinger M, Feldman Y (1996) Time domain dielectric spectroscopy study of human cells. I. Erythrocytes and ghosts. Biochim Biophys Acta 1280(1):34–40
70. McAdams ET, Jossinet J (1995) Tissue impedance – a historical overview. Physiol Meas 16:A1–A13

71. McGuinness R (2007) Impedance-based cellular assay technologies: recent advances, future promise. Curr Opin Pharmacol 7(5):535–540
72. Melin J, Jarvius J, Larsson C, Soderberg O, Landegren U, Nilsson M (2008) Ligation-based molecular tools for lab-on-a-chip devices. N Biotechnol 25(1):42–48
73. Mergel D, Buschendorf D, Eggert S, Grammes R, Samset B (2000) Density and refractive index of TiO2 films prepared by reactive evaporation. Thin Solid Films 371(1–2): 218–224
74. Metikoshukovic M, Babic R, Grubac Z, Brinic S (1994) Impedance spectroscopic study of aluminum and al-alloys in acid-solution – inhibitory-action of nitrogen-containing compounds. J. Appl Electrochem 24(8):772–778
75. Morita S, Umakoshi H, Kuboi R (1999) Characterization and on-line monitoring of cell disruption and lysis using dielectric measurement. J Biosci Bioeng 88(1):78–84
76. Naito S, Hoshi M, Mashimo S (1997) In vivo dielectric analysis of free water content of biomaterials by time domain reflectometry. Anal Biochem 251(2):163–172
77. Nandi N, Bhattacharyya K, Bagchi B (2000) Dielectric relaxation and solvation dynamics of water in complex chemical and biological systems. Chem Rev 100(6):2013–2045
78. Oleinikova A, Sasisanker P, Weingartner H (2004) What can really be learned from dielectric spectroscopy of protein solutions? A case study of ribonuclease A. J Phys Chem B 108(24):8467–8474
79. Oltrup T, Bende T, Kramer KD, Jean B (1999) Dielectric spectroscopy for noninvasive examination of corneal tissue. Biomed Tech (Berl) 44(4):78–82
80. Pal S, Bagchi B, Balasubramanian S (2005) Hydration layer of a cationic micelle, C(10)TAB: structure, rigidity, slow reorientation, hydrogen bond lifetime, and solvation dynamics. J Phys Chem B 109(26):12879–12890
81. Panda PK (2009) Review: environmental friendly lead-free piezoelectric materials. J Mater Sci 44(19):5049–5062
82. Park JH, Kim CS, Choi BC, Ham KY (2003) The correlation of the complex dielectric constant and blood glucose at low frequency. Biosens Bioelectron 19(4):321–324
83. Parsegian A (2005) Van der Waals forces – a handbook for biologists, chemists, engineers, and physicists. Cambridge University Press, Cambridge
84. Patel P, Markx GH (2008) Dielectric measurement of cell death. Enzyme Microb Technol 43(7):463–470
85. Pauly H (1966) Dielectric properties and ion mobility in erythrocytes. Biophys J (6):621–639
86. Pauly H, Schwan HP (1966) Dielectric properties and ion mobility in erythrocytes. Biophys J 6(5):621–639
87. Pearson DS, Smith G (1998) Dielectric analysis as a tool for investigating the lyophilization of proteins. PSTT 1(3):108–117
88. Pethrick RA (2002) Molecular motion in polymer systems. Curr Opin Solid State Mat Sci 6(3):221–225
89. Pickwell E, Wallace VP (2006) Biomedical applications of terahertz technology. J Phys D-Appl Phys 39(17):R301–R310
90. Polevaya Y, Ermolina I, Schlesinger M, Ginzburg BZ, Feldman Y (1999) Time domain dielectric spectroscopy study of human cells. II. Normal and malignant white blood cells. Biochim Biophys Acta 1419(2):257–271
91. Polk C, Postow E (ed) (1996) Handbook of biological effects of electromagnetic fields, 2nd edn. CRC Press, Boca Raton, FL
92. Powles JG (1951) The interpretation of dielectric measurements using the Cole-Cole plot. Proc Phys Soc Lon B 64(373):81–82
93. Prieve DC (2004) Changes in zeta potential caused by a dc electric current for thin double layers. Colloid Surf A Physicochem Eng Asp 250(1–3):67–77
94. Prodan C, Prodan E (1999) The dielectric behaviour of living cell suspensions. J Phys D-Appl Phys 32(3):335–343

95. Prodan E, Prodan C, Miller JH (2008) The dielectric response of spherical live cells in suspension: an analytic solution. Biophys J 95(9):4174–4182
96. Raicu V (1999) Dielectric dispersion of biological matter: model combing Debye-type and "universal" responses. Phys Rev 60(4):4678–4680
97. Rasaiah JC (1973) A view of electrolyte solutions. J Solution Chem 2(2–3):301–334
98. Resetic A, Babic R, Metikoshukovic M (1993) The electric and dielectric-properties of a coal-tar epoxy coating. Thin Solid Films 230(2):128–132
99. Resta R, Vanderbilt D (2007) Theory of polarization: a modern approach. In Physics of ferroelectrics: a modern perspective, vol 105. Springer, Berlin, pp 31–68
100. Ross DK (1968) Dipole moment of water in first hydration shell of a monovalent ion. Can J Phys 46(21):2407–2411
101. Rumenapp C, Remm M, Wolf B, Gleich B (2009) Improved method for impedance measurements of mammalian cells. Biosens Bioelectron 24(9):2915–2919
102. Sakmann B, Neher E (1984) Patch clamp techniques for studying ionic channels in excitable-membranes. Annu Rev Physiol 46:455–472
103. Salou P, Mejdoubi A, Brosseau C (2009) Modeling of the dielectric relaxation in eukaryotic cells. J Appl Phys 105(11):8
104. Schaefer M, Gross W, Ackemann J, Gebhard MM (2002) The complex dielectric spectrum of heart tissue during ischemia. Bioelectrochemistry 58(2):171–180
105. Schulze H, Giraud G, Crain J, Bachmann TT (2009) Multiplexed optical pathogen detection with lab-on-a-chip devices. J Biophotonics 2(4):199–211
106. Schwan HP (1957) Electrical properties of tissue and cell suspensions. Adv Biol Med Phys (5):147–209
107. Schwan HP (1988) Dielectric-spectroscopy and electro-rotation of biological cells. Ferroelectrics 86:205–223
108. Schwan HP (1993) Mechanisms responsible for electrical-properties of tissues and cell-suspensions. Med Prog Technol 19(4):163–165
109. Schwan HP (1999) The practical success of impedance techniques from an historical perspective. In: Riu PJ, Rosell J, Bragos R, Casas O (eds) Electrical bioimpedance methods: applications to medicine and biotechnology, vol 873. New York Acad Sciences, New York, NY, pp 1–12
110. Schwan HP (2000) Dielectric spectroscopy of biological materials and field interactions: the connection with Gerhard Schwarz. Biophys Chem 85(2–3):273–278
111. Schwan HP, Foster KR (1980) Rf-field interactions with biological-systems – electrical-properties and biophysical mechanisms. Proc IEEE 68(1):104–113
112. Schwan HP, Schwarz G, Maczuk J, Pauly H (1962) On the low-frequency dielectric dispersion of colloidal particles in electrolyte solution. J Phys Chem 66(12): 2626–2635
113. Schwan HP, Sheppard RJ, Grant EH (1976) Complex permittivity of water at 25°C. J Chem Phys 64(5):2257–2258
114. Schwan HP, Takashim S, Miyamoto VK, Stoecken W (1970) Electrical properties of phospholipid vesicles. Biophys J 10(11):1102–1119
115. Schwarz G (1962) A theory of the low-frequency dielectric dispersion of colloidal particles in electrolyte solution. J Phys Chem 66(12):2636–2642
116. Sen AD, Anicich VG, Arakelian T (1992) Dielectric-constant of liquid alkanes and hydrocarbon mixtures. J Phys D-Appl Phys 25(3):516–521
117. Shannon RD (1993) Dielectric polarizabilities of ions in oxides and fluorides. J Appl Phys 73(1):348–366
118. Simon GP (1994) Dielectric-relaxation spectroscopy of thermoplastic polymers and blends. Mater Forum 18:235–264
119. Smith G, Duffy AP, Shen J, Olliff CJ (1995) Dielectric relaxation spectroscopy and some applications in the pharmaceutical sciences. J Pharm Sci 84(9):1029–1044

120. Son JH (2009) Terahertz electromagnetic interactions with biological matter and their applications. J Appl Phys 105(10):10–15
121. South GP, Grant EH (1972) Dielectric dispersion and dipole-moment of myoglobin in water. Proc R Soc London, A 328(1574):371
122. Springer Handbook of Nanotechnology (2007) (2nd revised and extended edition) Springer, Berlin
123. Sun WQ (2000) Dielectric relaxation of water and water-plasticized biomolecules in relation to cellular water organization, cytoplasmic viscosity, and desiccation tolerance in recalcitrant seed tissues. Plant Physiol 124(3):1203–1215
124. Takashima S, Schwan HP (1985) Alignment of microscopic particles in electric-fields and its biological implications. Biophys J 47(4):513–518
125. Talary MS, Dewarrat F, Huber D, Falco-Jonasson L, Caduff A (2007) Non-invasive impedance based continuous glucose monitoring system. In: Scharfetter H, Merwa R (eds) 13th International Conference on Electrical Bioimpedance and the 8th Conference on Electrical Impedance Tomography 2007, vol 17. Springer, New York, NY, pp 636–639
126. Taylor K, van der Weide D (2002) Microwave assay for detecting protein conformation in solution. In: Jensen JO, Spellicy RL (eds) Instrumentation for air pollution and global atmospheric monitoring, vol 4574. Spie-Int Soc Optical Engineering, Bellingham, pp 137–143
127. Teixeira AP, Oliveira R, Alves PM, Carrondo MJT (2009) Advances in on-line monitoring and control of mammalian cell cultures: supporting the PAT initiative. Biotechnol Adv 27(6):726–732
128. Tirado MC, Arroyo FJ, Delgado AV, Grosse C (2000) Measurement of the low-frequency dielectric properties of colloidal suspensions: comparison between different methods. J Colloid Interface Sci 227(1):141–146
129. Tura A, Sbrignadello S, Barison S, Conti S, Pacini G (2007) Dielectric properties of water and blood samples with glucose at different concentrations. In: Jarm T, Kramar P, Zupanic A (eds) 11th Mediterranean Conference on medical and biological engineering and computing 2007, vols 1 and 2, vol 16. Springer, Berlin, pp 194–197
130. Tura A, Sbrignadello S, Barison S, Conti S, Pacini G (2007) Impedance spectroscopy of solutions at physiological glucose concentrations. Biophys Chem 129(2–3):235–241
131. Valentinuzzi ME, Morucci JP, Felice CJ (1996) Bioelectrical impedance techniques in medicine .2. Monitoring of physiological events by impedance. Crit Rev Biomed Eng 24(4–6):353–466
132. Varshney M, Li YB (2009) Interdigitated array microelectrodes based impedance biosensors for detection of bacterial cells. Biosens Bioelectron 24(10):2951–2960
133. Vermoyal JJ, Frichet A, Dessemond L, Hammou A (1999) AC impedance study of corrosion films formed on zirconium based alloys. Electrochim Acta 45(7):1039–1048
134. Wu JF, Yuan XZ, Wang HJ, Blanco M, Martin JJ, Zhang JJ (2008) Diagnostic tools in PEM fuel cell research: part I – Electrochemical techniques. Int J Hydrog Energy 33(6): 1735–1746
135. Xu D, Phillips JC, Schulten K (1996) Protein response to external electric fields: relaxation, hysteresis, and echo. J Phys Chem 100(29):12108–12121
136. Yuan XZ, Wang HJ, Sun JC, Zhang JJ (2007) AC impedance technique in PEM fuel cell diagnosis – a review. Int J Hydrog Energy 32(17):4365–4380
137. Zhang MIN, Repo T, Willison JHM, Sutinen S (1995) Electrical-impedance analysis in plant-tissues – on the biological meaning of Cole-Cole-alpha in scots pine needles. Eur Biophys J 24(2):99–106
138. Zhou H, Preston MA, Tilton RD, White LR (2005) Calculation of the dynamic impedance of the double layer on a planar electrode by the theory of electrokinetics. J Colloid Interface Sci 292(1):277–289
139. Zou Y, Guo Z (2003) A review of electrical impedance techniques for breast cancer detection. Med Eng Phys 25(2):79–90